OPEN ACCESS
The Journal of Engineering and Exact Sciences – jCEC, Vol. 10 N. 01 (2024)
journal homepage: https://periodicos.ufv.br/jcec
eISSN: 2527-1075
ISSN: 2446-9416

Predictive Control for PV- Water Pumping System based of Interconnected High Gain Observer

Article Info:
Article history: Received 2023-09-09 / Accepted 2024-01-04 / Available online 2024-01-06
doi: 10.18540/jcecvl10iss1pp18214

Lamouchi Zakaria
ORCID: https://orcid.org/0000-0003-2240-3540
Faculty of Technology, University of El-Oued, 3900 El Oued, Algeria
E-mail: prof_lammouchi@yahoo.fr
Allal Abderrahim
ORCID: https://orcid.org/0000-0002-7382-5180
Faculty of Technology, University of El-Oued, 3900 El Oued, Algeria
E-mail: allalabderrahim@yahoo.fr
Khechekhouche Abderrahmane
ORCID: https://orcid.org/0000-0002-7278-2625
Faculty of Technology, University of El-Oued, 3900 El Oued, Algeria
E-mail: abder03@hotmail.com
Antonio Marcos de OliveiraSiqueira
ORCID: https://orcid.org/0000-0001-9334-0394
Universidade Federal de Viçosa, Brazil
E-mail: antonio.siqueira@ufv.br
Julio César Costa Campos
ORCID: https://orcid.org/0000-0002-9488-8164
Universidade Federal de Viçosa, Brazil
E-mail: julio.campos@ufv.br
Kheireddine Lamamra
ORCID: https://orcid.org/0000-0002-9867-8463
Laboratory LENT, University of Oum El Bouaghi, Algeria
E-mail: lamamra.kheireddine@univ-oeb.dz

Abstract

This article presents a comprehensive evaluation of an integrated photovoltaic (PV) and water pumping system employing both Finite Set Model Predictive Control (FS-MPC) and Deat Beat Predictive Control (DB-MPC) under varying insolation levels (1000 W/m² to 700 W/m²). The system, initially tested at 1000 W/m², rapidly achieves Maximum Power Point Tracking (MPPT), stabilizing PV parameters at the MPP within 0.2 seconds. Notably, DB-MPC demonstrates superior dynamic response and faster settling times compared to conventional methods. The Interconnected High-Gain Observer accurately estimates motor speed, facilitating the attainment of the rated rotor speed in line with the desired reference speed. Transitioning from 1000 W/m² to 700 W/m² insolation, the system exhibits stability in V_{pv} and rapid I_{pv} adjustment at MPP. The InC algorithm extends PV array operation, showcasing a decrease in power output to 2204 W at 60% flow rate. These results affirm the efficacy and adaptability of the proposed control strategies in optimizing the performance of the PV-driven water pumping system, offering promising advancements in sustainable energy applications.

Keywords: Photovoltaic. Incremental conductance. Induction Motor Drive. Water Pump. Conventional control. Deatbeat Predictive Control. Cost function. High gain observer.

1. Introduction

The advantages of using photovoltaic (PV) energy in the field of water pumping are the ease of assembly and installation of the elements, lower maintenance and noise-free operation (no moving parts) (Keshavarzi *et al.*, 2021). Generally, the PV system consists of three parts: PV array, converters and group of motor-pumps (Shukla *et al.*, 2020). A DC motor was the first motor used for PV water pumping. However, with virtues related to the induction motor (IM), it has replaced the DC motor (Singh *et al.*, 2018). As the research progressed, many structures related to the PV system emerged. The single-phase topology was used with a single converter instead of two converters to control the DC-link voltage and Maximum Power Point Tracking (MPPT) (Lakshmi *et al.*, 2019; Mathew *et al.*, 2023).

Maximum power extraction techniques have played a part in scientific research. Therefore, different techniques have been developed in order to work at the MPPT, which differ in their complexity, speed and precision when tracing this point (Kumar *et al.*, 2023; Rosas-Caro *et al.*, 2023). Few published works in the literature have developed and improved incremental-conductance algorithms (InC) as per consumers' requirements. Here, an InC-based MPPT algorithm is applied with a derating mechanism, which is eligible to regulate the flow rate corresponding to the desired flow (Shang *et al.*, 2020). The FS-MPC predictive control strategy has spread, which has produced different ideas on the one hand, and it is characterized by very simple and very good performance on the other hand (Comarella *et al.*, 2023; Kanaan *et al.*, 2020). The principle of FS-MPC is to select the optimal vector that corresponds to the reduced cost function (Lammouchi *et al.*, 2020a).

In general, in order to choose the optimum voltage vector, all possible vectors must be considered, eight switching states for two-level (2-L) inverter (Lammouchi *et al.*, 2020b; Wang *et al.*, 2022). On the other hand, two or more terms are used in the cost function. The balance between these terms is achieved through weighting factors. These factors are calculated either experimentally or by inaccurate applications (Luo *et al.*, 2023; Murillo-Yarce *et al.*, 2023). It takes a very time-consuming and complex to find these factors which make this task very difficult. Several studies have been conducted in recent years to solve the weight factors problem in the complex cost function. In (Xie *et al.*, 2021), the authors proposed dividing the compound cost function into multiple functions to avoid the weight factor. On the other hand, authors in (Bekhoucha *et al.*, 2021) proposed a DB-MPC for the synchronous machine, in this research, the cost function is represented by minimizing the tracking error for one variable related to stator voltage. Several efforts have focused to control of IM without a mechanical sensor (El Daoudi *et al.*, 2021; El Ouanjli *et al.*, 2022). Authors in (Traore *et al.*, 2012) propose an interconnected observer to estimate the state of IM using stator currents and voltages. The idea is to design an observer for the whole system by connecting two subsystems extracted from the whole motor model (Zhang *et al.*, 2020).

This study improves the high-gain observer for induction motor (IM) in water pumping, estimating speed, load torque, and flux from stator voltage and current. Objectives include designing a single-stage PV array without a DC-DC converter, using Incremental-Conductance Algorithm for reference speed, implementing Predictive Control (FS-MPC), introducing Deatbeat Predictive Control (DB-MPC) to simplify factor selection, and utilizing a high-gain observer for IM-Pump speed estimation. Simulation results confirm the effectiveness of these methods, demonstrating enhanced performance for water pumping applications.

2. System architecture

Figure 1 shows the application of predictive control strategy to a gross system consisting of a simplified PV array linked with an IM-Pump. FS-MPC technique generates the gating signals to a three-phase inverter, eliminating the need for any intermediary modulator. Current and voltage sensors are used to estimate the speed of motor by an interconnected observer. An InC algorithm is exercised for MPPT for high power extraction.

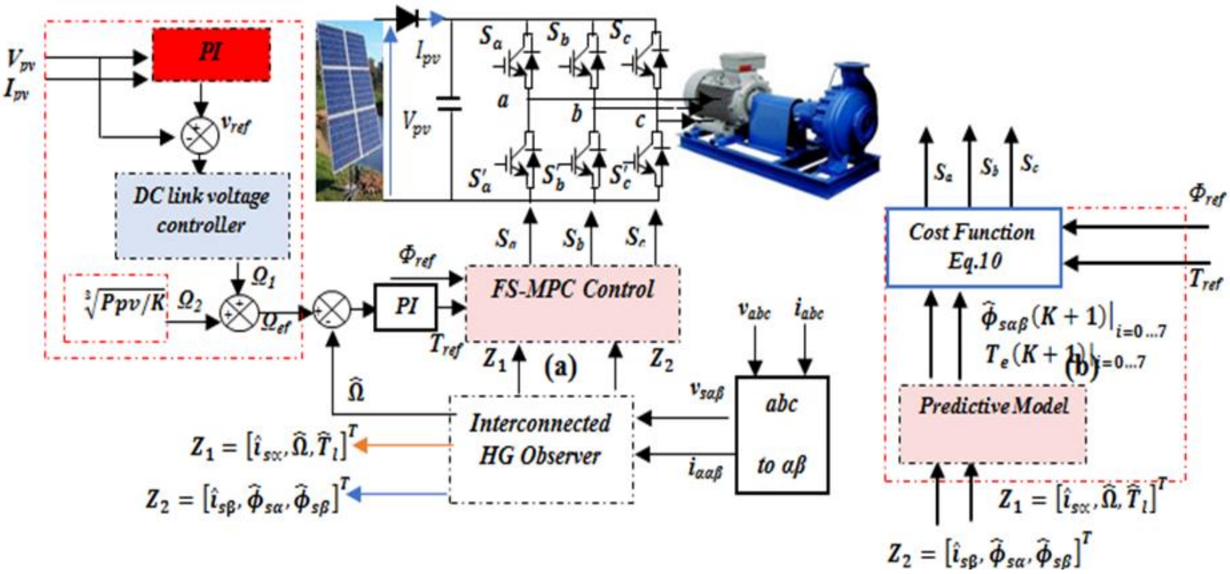

Figure 1. Diagram of single stage PV system powered IM drive. (a): global system (b): FS-MPC control.

1.1. Design of PV Array

In this work, a 3.4 kW motor is used and connected to a 3.7 kW PV array. The specifications of PV array used in this work are summarized in Table 1. Table 2 represents the parameters of the induction motor needed in this study.

Table 1. Specifications of used PV array.

Maximum Voltage at MPP	537V
Maximum Power at MPP	3700W
Current at MPP,	7.63A
Number parallel and series of module	31,12
Current Isc	7.68
Voltage Voc	650

Table 2. Induction Motor Parameters.

Rated speed	Ω =1445 tr/mn
Rated torque	T_e =23 N.m
Stator resistance	R_s=0.7384 Ω
Rotor resistance	R_r= 0.7043Ω
Rotor inductance	L_r = 0.165 H
Stator inductance	L_s =0.161 H
Inertia moment	J =0.0343 kg-m^2
Mutual inductance	M= 0.155H

2.2 Determination of DC-Link voltage

One of the conditions for controlling the inverter's (output current) is the amplitude of input voltage. Its value should be higher than the line voltage value of the motor (Khan *et al.*, 2019; Khodapanah *et al.*, 2023). The value of the DC-Link voltage is given as:

$$V_{dc} > \sqrt{2} * V_l = \sqrt{2} * 380 = 537\ V \quad (1)$$

Hence, after taking the relation between the voltage and the capacitor of the dc-link, the suitable value of this capacitor is determined as 2500 μF.

2.3 Reference speed

Reference speed can be obtained by using (2) and (3) as follows:

$$\varepsilon_{vdc}(k) = V_{dc}^{*}(k) - V_{PV}(k) \tag{2}$$

$$\Omega_1(k) = \Omega_1(k-1) + K_{Pdc}\left(\varepsilon_{vdc}(k) - \varepsilon_{vdc}(k-1)\right) + K_{Idc}\varepsilon_{vdc}(k) \tag{3}$$

It can get the reference speed (Ω_{ref}) from a PI controller. However, the dynamic response of the system in this case is very weak. In order to obtain a fast dynamic response, another speed is used with Ω_1 (by instantaneous reflection of the PV energy on the motor speed). To derive the second speed Ω_{PV}, we use the pump convergence law by the following formula:

$$\Omega_{PV}(k) = \left(P_{PV}(k)/K_{Pm}\right)^{1/3} \tag{4}$$

where, K_{pm} is the proportional gain. From (3) and (4), the reference speed is given by:

$$\Omega_{ref}(k) = \Omega_1(k) + \Omega_{PV}(k) \tag{5}$$

2.4 InC algorithm

InC algorithm, MPPT control strategy can be modified to some extent by operating the PV array at various operating point (10% to 100%) of rated insolation. The idea came from the point of view of domestic water consumption, where consumers can request smaller amounts of water drainage. According to the famous equation, the solution can be found by integrating a single flow control loop with a MPPT algorithm and configuring a fixed duty cycle that aligns with the desired flow rate, as shown in Figure 2.

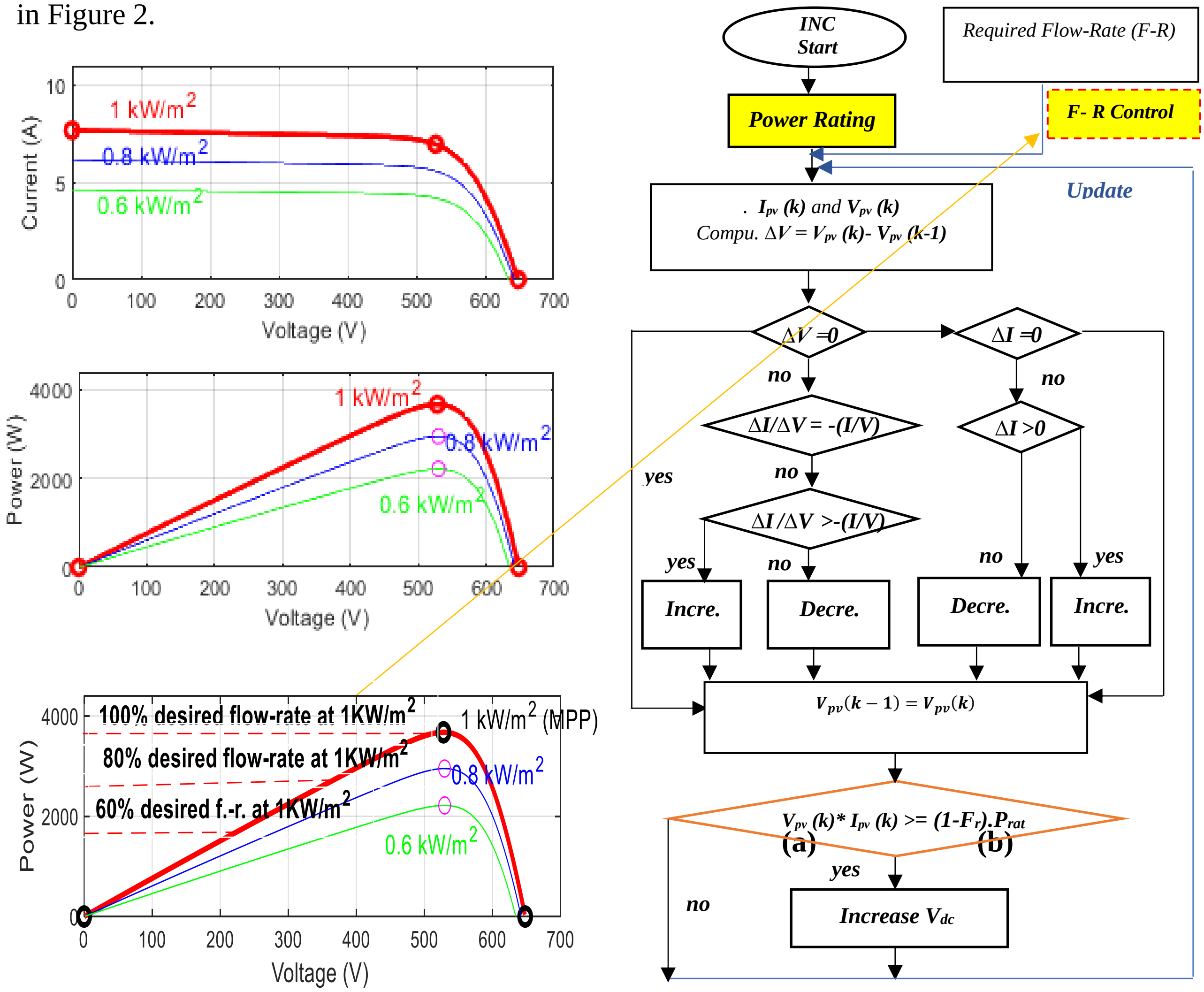

Figure 2. InC. Strategy (a) Curve of *PV Array (b)* . InC. Algorithm.

2.5 Load Torque

In this work, the motor speed and load torque have a non-linear relationship. This relation is obtained as follows:

$$T_l = K_1 \Omega^2 \quad (6)$$

where, K_1 is a proportional gain.

2.6 Induction Motor model

Mathematical model of the IM is given in the frame of reference (α-β), the load torque is added in state variables. The load torque equation this is obtained by (6), the full model of IM is given as:

$$\begin{pmatrix} i_{s\alpha} \\ i_{s\beta} \\ \dot{\phi}_{r\alpha} \\ \dot{\phi}_{r\beta} \\ \dot{\Omega} \\ \dot{T}_L \end{pmatrix} = \begin{pmatrix} -F_1 i_{r\alpha} - F_2\phi_{r\alpha} + F_3\Omega\phi_{r\beta} \\ -F_1 i_{r\beta} - F_3\Omega\phi_{r\alpha} + F_2\phi_{r\beta} \\ F_4 i_{r\alpha} - F_5\phi_{r\alpha} - p\Omega\phi_{r\beta} \\ F_4 i_{r\beta} + p\Omega\phi_{r\alpha} - F_5\phi_{r\beta} \\ F_6(\phi_{r\alpha} i_{r\beta} - \phi_{r\beta} i_{r\alpha}) - F_7\Omega - F_8 T_L \\ F_9\Omega \end{pmatrix} + \begin{pmatrix} F_{10} & 0 \\ 0 & F_{10} \\ 0 & 0 \\ 0 & 0 \\ 0 & 0 \\ 0 & 0 \end{pmatrix} \begin{pmatrix} V_{s\alpha} \\ V_{s\beta} \end{pmatrix} \quad (7)$$

where, $F_1 = \frac{1}{\sigma L_s}\left(R_s + \frac{L_m^2}{T_r L_r}\right)$, $F_2 = \frac{1}{\sigma L_s}\left(\frac{L_m}{T_r L_r}\right)$, $F_3 = \frac{p}{\sigma L_s}\left(\frac{L_m}{L_r}\right)$, $F_4 = \left(\frac{L_m}{T_r}\right)$, $F_5 = \left(\frac{1}{T_r}\right)$,
$F_6 = \left(\frac{pL_m}{JL_r}\right)$, $F_7 = \left(\frac{f_v}{J}\right)$, $F_8 = \left(\frac{1}{J}\right)$, $F_9 = 2.K_1$, $F_{10} = \frac{1}{\sigma L_s}$, $\sigma = 1 - \left(\frac{L_m^2}{L_s L_r}\right)$, $T_r = \left(\frac{L_r}{R_r}\right)$,

The parameters R_r and R_s are rotor and stator resistances, respectively. L_r, L_s and L_m) are rotor, stator and mutual inductances, respectively. p is the number of pole pairs. The parameter values of the IM are shown in Table 1S.

2.7 Conventional predictive FS-MPC control

The conventional FS-MPC of the studied system is presented in Figure 1(b). The switching states S and the output voltage V_s can be expressed as:

$$S = \frac{3}{2}(S_a + e^{j2\pi/3}S_b + e^{j4\pi/3}S_c) \quad (8)$$

$$V_s(S_{a,b,c}) = \sqrt{\frac{2}{3}}\frac{V_{dc}}{2}(S_a + e^{j2\pi/3}S_b + e^{j4\pi/3}S_c) \quad (9)$$

On the other hand, the torque and stator flux are directly controlled using the cost function in (10)

$$F_{|i=1:8} = abs\left(T_e^* - T_e^p(k+1)\right) - \gamma_\psi * \ abs\left(\Phi_s^* - \ \Phi_s^p(k+1)\right) \quad (10)$$

where γ_ψ is the weighting factor which denotes the balance between parameters control in the cost function.

The discrete model of IM in (7) is obtained by (11) using the forward Euler approximation (Lammouchi & Barra, 2020; Su et al., 2017):

$$\begin{cases} \phi_s(k+1) = \phi_s(k) + T_s V_s(k+1) - R_s I_s(k) \\ i_s(k+1) = \left(1 - \frac{T_s R_\tau}{L_s \sigma}\right) i_s(k) + \left((\tau_r k_r - jk_r\Omega)\phi_s(k) + V_s(k+1)\right) \\ T_e(k+1) = \frac{3}{2}p\phi_s(k+1).\, i_s(k+1) \end{cases} \quad (11)$$

From (10) and (11), using the conventional FS-MPC, it can be seen the balance between terms in cost function is achieved through weighting factors. These factors are calculated either experimentally or by inaccurate applications. It takes a very time-consuming and complex to find these factors which make this task very difficult. To solve this problem, a DB-MPC control is suggested.

3. DB-MPC Control

As previously mentioned, the stator torque and flux are directly controlled in FS-MPC using a cost function. On the other hand, the torque is calculated from the stator q-axis current reference i_{sq}^* and obtained by the output of speed controller, while the component of the stator current i_{sd}^* is set as a constant value because it is the flux-producing component (Sandre Hernandez *et al.*, 2021). Assuming the DB-MPC is working properly at the time $(k + 1)$ so:

$$\left\| \begin{array}{l} i_{sd}(k+1) = i_{sd}^* \\ i_{sq}(k+1) = i_{sq}^* \end{array} \right. \tag{12}$$

According to (7), the reference voltages (V_{sd}^*, V_{sq}^*) can be written as follows:

$$V_{Sd}^* = \frac{1}{F_{10}}\left(\left(\frac{i_{sd}^* - i_{sd}(k)}{T_s}\right) + F_1.i_{sd}(k) - \Omega_s.i_{sq}(k) - F_2.\phi_{rd}(k) - F_3.\Omega(k).\phi_{rq}(k)\right)$$

$$V_{Sq}^* = \frac{1}{F_{10}}\left(\left(\frac{i_{sq}^* - i_{sq}(k)}{T_s}\right) - \Omega_s.i_{sd}(k) + F_1.i_{sq}(k) - F_2.\phi_{rq}(k) + F_3.\Omega(k).\phi_{rd}(k)\right) \tag{13}$$

The transformation of the reference voltage vector dq to $\alpha\beta$ frame expression can be obtained by:

$$\begin{pmatrix} V_{s\alpha}^* \\ V_{s\beta}^* \end{pmatrix} = \begin{pmatrix} cos\theta_e & -sin\theta_e \\ sin\theta_e & cos\theta_e \end{pmatrix}\begin{pmatrix} V_{sd}^* \\ V_{sq}^* \end{pmatrix} \tag{14}$$

The new cost function of the DB-MPC can be updated to obtain the optimal voltage vector, which is the difference between the reference vector and candidate vector as:

$$F_{|i=1:8} = abs\left(V_{s\alpha}^* - V_{s\alpha}^p(k+1)\right) + abs\left(V_{s\beta}^* - V_{s\beta}^p(k+1)\right) \tag{15}$$

4. Interconnected observer

The nonlinear system of induction motor model is difficult to find a suitable method to design an observer for the full system. To solve this problem, this paper proposes an interconnected observer between two subsystems of the full model of the motor-pump. It is satisfies some required properties. Hence, the states of each of the two systems are available for the other system, and with this aim, the model of induction motor, (7), can be rewritten into two interconnected systems:

$$\begin{bmatrix} \dot{i_{s\alpha}} \\ \dot{\Omega} \\ \dot{T_l} \end{bmatrix} = \begin{bmatrix} 0 & F_3\phi_{r\beta} & 0 \\ 0 & 0 & -F_8 \\ 0 & 0 & 0 \end{bmatrix}\begin{bmatrix} i_{s\alpha} \\ \Omega \\ T_l \end{bmatrix} + \begin{bmatrix} -F_1 i_{s\alpha} + F_2\phi_{r\alpha} + F_{10}V_{s\alpha} \\ F_6\left(\phi_{r\alpha}i_{s\beta} - \phi_{r\beta}i_{s\alpha}\right) - F_7\Omega \\ F_9\Omega \end{bmatrix} \tag{16}$$

$$\begin{bmatrix} \dot{i_{r\beta}} \\ \dot{\phi}_{r\alpha} \\ \dot{\phi}_{r\beta} \end{bmatrix} = \begin{bmatrix} -F_1 & -F_3\Omega & F_2 \\ 0 & -F_5 & -p\Omega \\ 0 & p\Omega & -F_5 \end{bmatrix}\begin{bmatrix} i_{s\beta} \\ \phi_{r\alpha} \\ \phi_{r\beta} \end{bmatrix} + \begin{bmatrix} F_{10}V_{s\beta} \\ F_4 i_{s\alpha} \\ F_4 i_{s\beta} \end{bmatrix} \tag{17}$$

The torque T_l represents the load torque, which is proportional to the square of the rated speed, as in (6). On the other hand, the rotor currents and stator voltages of the motor-pump system are measured.

The variables of two subsystems have been considered in order to separate the magnetic variables in one subsystem and the magnetic variables in the other one the mechanical variables.

$$\begin{array}{l} \dot{X}_1 = A_{hg1}(X_2)X_1 + g_{hg1}(u, y, X_2, X_1) \\ \qquad y_1 = C_1 X_1 \end{array} \tag{18}$$

$$\dot{X}_2 = A_{hg2}(X_1)X_2 + g_{hg2}(u,y) \qquad y_2 = C_2X_2 \tag{19}$$

Where $u = [V_{s\alpha} \;\; V_{s\beta}]'$ can be an input, $X_1 = [i_{s\alpha} \quad \Omega \quad T_l]'$, $X_2 = [i_{s\beta} \quad \phi_{r\alpha} \quad \phi_{r\beta}]'$, $y = [i_{s\alpha} \;\; i_{s\beta}]'$, $C_1 = C_2 = [1 \quad 0 \quad 0]'$.

$$A_{hg1} = \begin{bmatrix} 0 & F_3\phi_{r\beta} & 0 \\ 0 & 0 & -F_8 \\ 0 & 0 & 0 \end{bmatrix}, \qquad g_{hg1} = \begin{bmatrix} -F_1 i_{s\alpha} + F_2\phi_{r\alpha} + F_{10}V_{s\alpha} \\ F_6(\phi_{r\alpha} i_{s\beta} - \phi_{r\beta} i_{s\alpha}) - F_7\Omega \\ F_9\Omega \end{bmatrix}$$

$$A_{hg2} = \begin{bmatrix} -F_1 & F_3\Omega & F_2 \\ 0 & -F_5 & -p\Omega \\ 0 & p\Omega & -F_5 \end{bmatrix}, \qquad g_{hg2} = \begin{bmatrix} F_{10}V_{s\beta} \\ F_4 i_{s\alpha} \\ F_4 i_{s\beta} \end{bmatrix}$$

- A_{hg1} and A_{hg2} are globally Lipschitz with respect to X_2 and X_1 respectively.
- g_{hg1} is globally Lipschitz with respect to X_2 uniformly with respect to the pair (u, X_1).

Remark 1: The main objective is to design an enhanced interconnected high-gain observer for subsystems (18) and (19) by using measured currents and voltages for an IM- pump water.
The first observer, Figure 3 allows observing the speed and load torque of motor-pump while the second one is consecrated to estimate the rotor fluxes, the observer model can be written as:

$$\begin{cases} \dot{Z}_1 = A_{hg1}(Z_2)Z_1 + g_{hg1}(u,y,Z_2,Z_1) + S_1^{-1}C_1^T(y_1 - \hat{y}_1) \\ \dot{S}_1(\theta_1) = -\theta_1 S_1 - A_{hg1}^T(Z_2)S_1 - S_1 A_{hg1}(Z_2) + C_1^T C_1 \\ \hat{y}_1 = C_1 Z_1 \end{cases} \tag{20}$$

$$\begin{cases} \dot{Z}_2 = A_{hg2}(Z_1)Z_2 + g_{hg2}(u,y,Z_2,Z_1) + S_2^{-1}C_2^T(y_2 - \hat{y}_2) \\ \dot{S}_2(\theta_2) = -\theta_2 S_2 - A_{hg2}^T S_2 - S_2 A_{hg2} + C_2^T C_2 \\ \hat{y}_2 = C_2 Z_2 \end{cases} \tag{21}$$

where: $S_1^{-1}C_1^T$ and $S_2^{-1}C_2^T$ are the gains of the proposed observers. $Z_1 = [\hat{\imath}_{s\alpha} \quad \hat{\Omega} \quad \hat{T}_l]'$, $Z_2 = [\hat{\imath}_{s\beta} \quad \hat{\phi}_{r\alpha} \quad \hat{\phi}_{r\beta}]'$, $C_1 = C_2 = [1 \quad 0 \quad 0]'$, $u = [V_{r\alpha} \; V_{s\beta}]'$, $\hat{y}_1 = \hat{\imath}_{s\alpha}$ and $\hat{y}_2 = \hat{\imath}_{s\beta}$.
From (20) and (21), $\dot{S}_1$ and $\dot{S}_2$ can be rewritten as follows:

$$\dot{S}_1(\theta_1) = \begin{bmatrix} \dot{S}_{1,11} & \dot{S}_{1,12} & \dot{S}_{1,13} \\ 0 & \dot{S}_{1,22} & \dot{S}_{1,23} \\ 0 & 0 & \dot{S}_{1,33} \end{bmatrix}, \quad \dot{S}_2(\theta_2) = \begin{bmatrix} \dot{S}_{2,11} & \dot{S}_{2,12} & \dot{S}_{2,13} \\ 0 & \dot{S}_{2,22} & \dot{S}_{2,23} \\ 0 & 0 & \dot{S}_{2,33} \end{bmatrix} \tag{22}$$

where,

$$\begin{cases} \dot{S}_{1,11} = -\theta_1 S_{1,11} + 1 \\ \dot{S}_{1,12} = -\theta_1 S_{1,12} - F_3\phi_{r\beta} S_{1,11} \\ \dot{S}_{1,13} = -\theta_1 S_{1,13} + F_8 S_{1,12} \\ \dot{S}_{1,22} = -\theta_1 S_{1,22} - 2F_3\phi_{r\beta} S_{1,12} \\ \dot{S}_{1,23} = -\theta_1 S_{1,23} - F_3\phi_{r\beta} S_{1,13} + F_8 S_{1,22} \\ \dot{S}_{1,33} = -\theta_1 S_{1,33} + 2F_8 S_{1,23} \end{cases} \tag{23}$$

$$\begin{cases}\dot{S}_{2,11} = -\theta_2 S_{2,11} + 2F_1 S_{2,11} + 1 \\ \dot{S}_{2,12} = -\theta_2 S_{2,12} + (F_1 + F_5) S_{2,12} + F_3 \Omega S_{2,11} - 2\Omega S_{2,13} \\ \dot{S}_{2,13} = -\theta_2 S_{2,13} + F_2 S_{2,11} + (F_1 + F_5) S_{2,13} + 2\Omega S_{2,12} \\ \dot{S}_{2,22} = -\theta_2 S_{2,22} - 2F_5 S_{2,22} + 2F_3 \Omega S_{2,12} - 4\Omega S_{2,23} \\ \dot{S}_{2,23} = -\theta_2 S_{2,23} + 2F_5 S_{2,23} - F_2 S_{2,12} + F_3 \Omega S_{2,13} + 2\Omega S_{2,22} + 2\Omega S_{2,33} \\ \dot{S}_{2,33} = -\theta_2 S_{2,33} + 2F_5 S_{2,33} - 2F_2 S_{2,13} + 4\Omega S_{2,23}\end{cases} \quad (24)$$

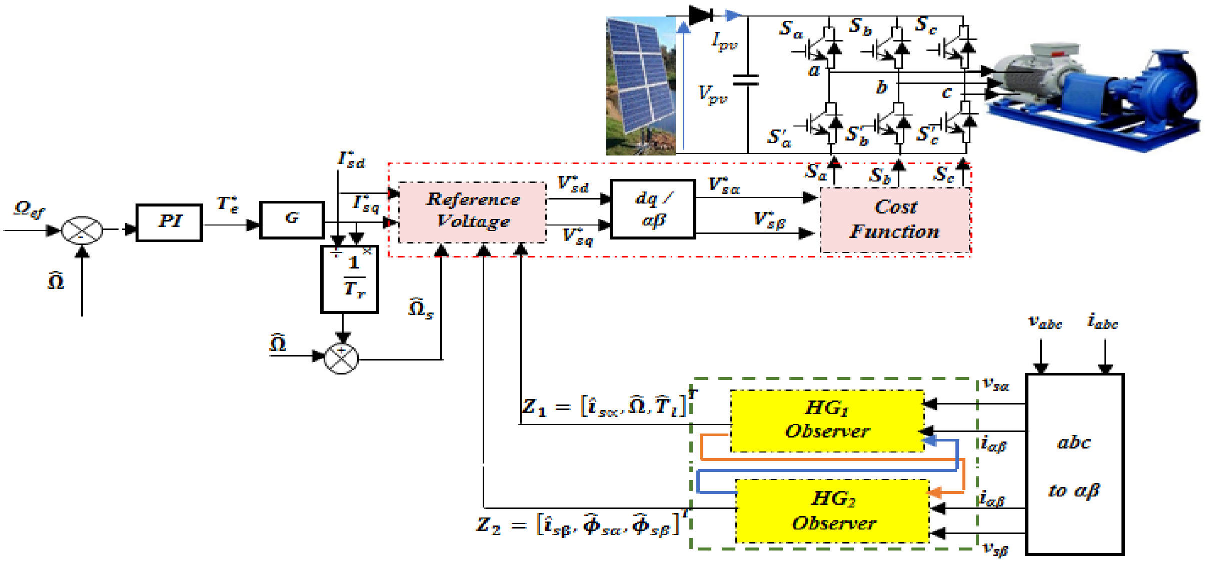

Figure 3. Diagram of single stage PV powered IM with DB -MPC based of High Gain interconnected observer

Remark 2: It is important to emphasize that the observability conditions for this observer have been carefully studied in (Ghanes *et al.*, 2005; Naifar *et al.*, 2015). To guarantee the convergence of this observer, specific conditions have been established, requiring that both θ_1 and θ_2 are sufficiently positive values

5. Simulation results

5.1. Predictive control performance over different levels of radiation

Figure 4 shows the performance of the whole system, PV with water pumping system using FS-MPC and DB-MPC at different levels of insolation from 1000 W/m^2 to 700 W/m^2. The system is initially tested directly at 1000 W/m^2. When the system is running, MPPT is quickly reached. Figure 3 shows an increase of photovoltaic power (P_{pv}) and PV voltage (V_{pv}), which stabilizes this values (V_{pv}, I_{pv} and P_{pv}) at maximum MPP point within fraction of second (about 0.2s). The Figures show the performance of the whole system (PV system with motor-pump) at 1000 W / m^2 insolation by applying predictive control techniques (FS-MPC and DB -MPC) and At 0.75 seconds, the MPP is moved to the new points where the insolation level changes to 700 W/m^2, there is slight change in the voltage V_{pv} at maximum power however, the current I_{pv} at MPP change significantly. Once MPP is tracked, the technique MPPT (InC) for controlling the Vpv maintains it at the same point.

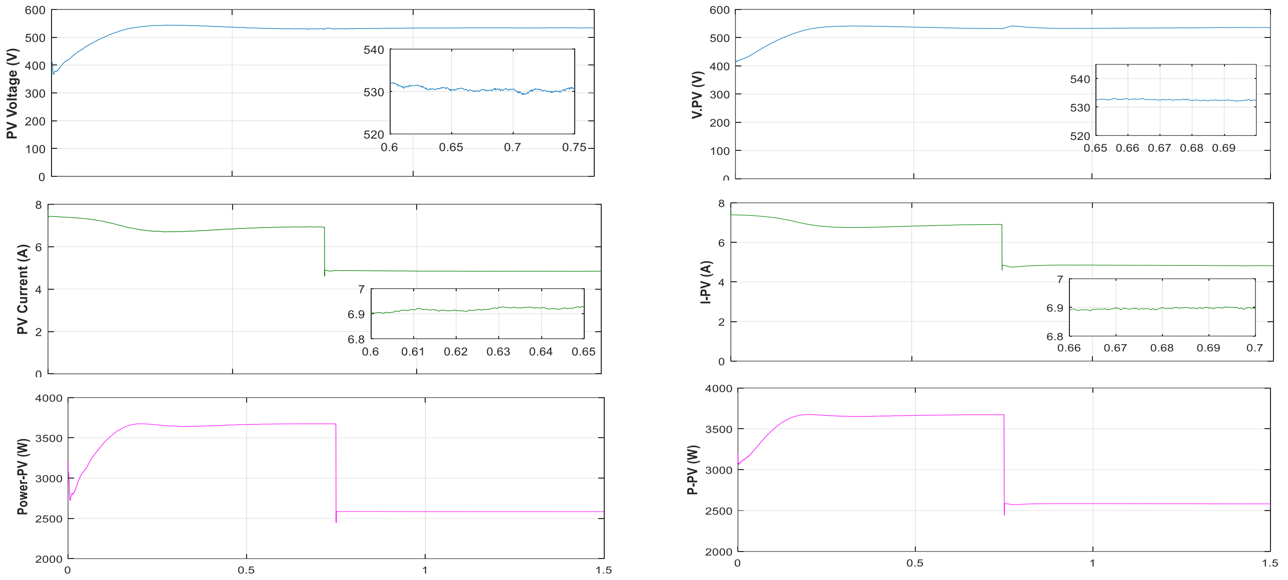

(a) (b)

Figure 4. Dynamic of the PV system when insolation level drops from 1000 to 700W/m² with FS-MPC and DB-MPC.

Figure 5 presents motor speed (ω_m), flux , the stationery currents components ($i_{s\alpha}$ and $i_{s\beta}$), the electromagnetic torque (T_e) and the pump torque (T_p). We were able to estimate the motor speed using the interconnected high gain observer. From Figure6, the starting performance of IM is tested at 1000 W/m^2. The MPPT algorithm determines the reference speed. The results show the induction motor drive rapidly attains its rated rotor speed (Ω) in accordance with the desired reference speed (152rd/s). The stationery currents components are ($i_{s\alpha}$ and $i_{s\beta}$), the electromagnetic torque (T_e) reached a value of 23 N.m very quickly, as it represents the steady-state value.

In Figure 5, both speeds (ω_{sen}) and (ω_m) align during the steady-state at 1000 W/m². The torque (T_e) quickly stabilizes at 23 N.m. The reference speed shifts to approximately 135 (rad/s) at 0.75 seconds due to changing insolation to 700 W/m², showcasing the rapid motor speed response with DB-MPC control. This change corresponds to a variation in the load torque T_p (pump torque), influencing the motor's phase current and electromagnetic torque T_e, settling at a new level.

The DB predictive controller demonstrates the fastest dynamic response and lowest settling time compared to conventional methods.

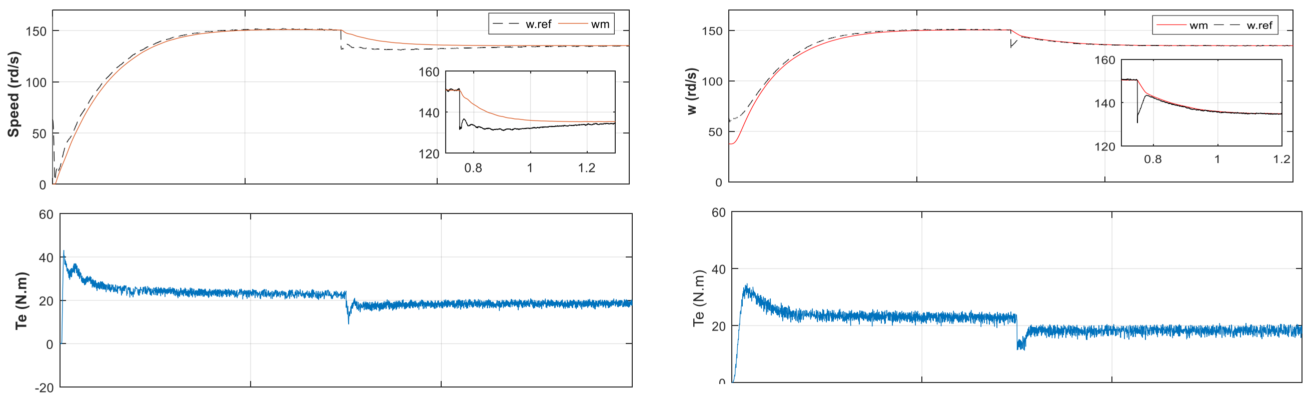

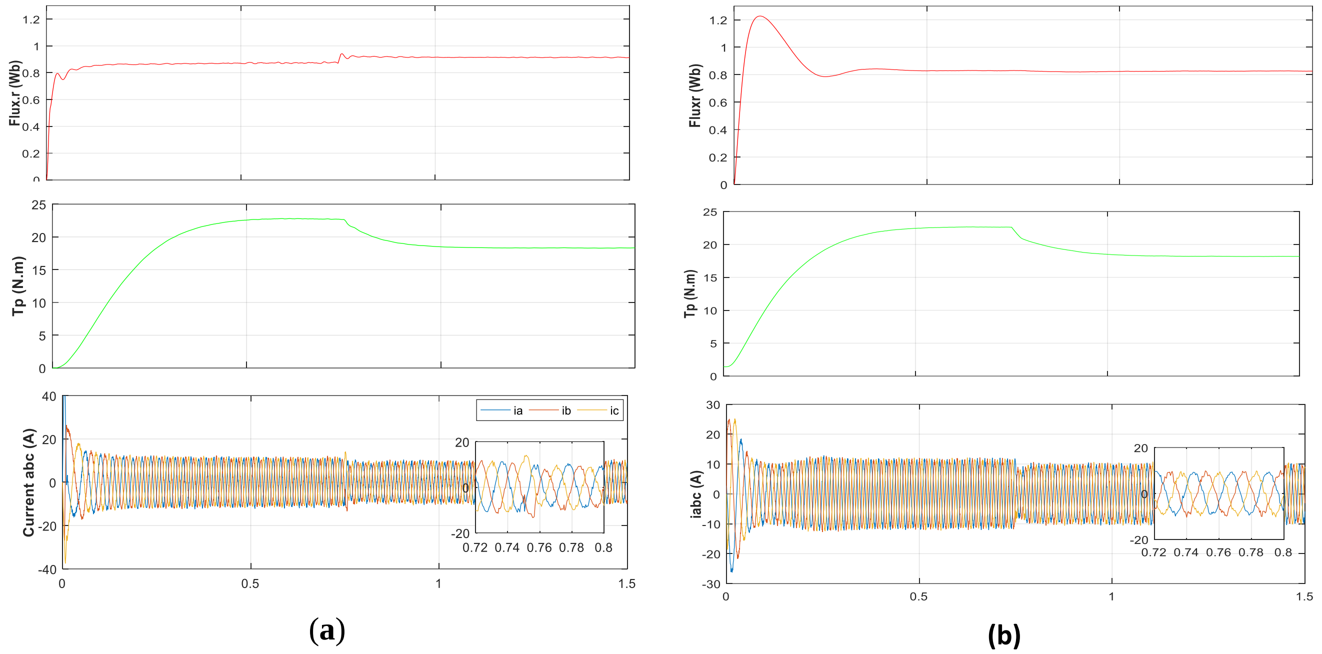

Figure 5. Dynamic of induction motor when insolation level drops from 1000 to 700W/m²
(with FS-MPC and DB3-MPC).

5.2 *Desired Flow Rate Control*

The developed InC algorithm is extended by running the photovoltaic array at different operating points with a constant insolation. From Figure 6, the insolation is 1000 W/m^2. It is noticed a decrease in the photovoltaic power output to the values 2204 W corresponding to the desired flow rate at 60%, the speed of the motor and the torque are obtained corresponding to the values at this request point.

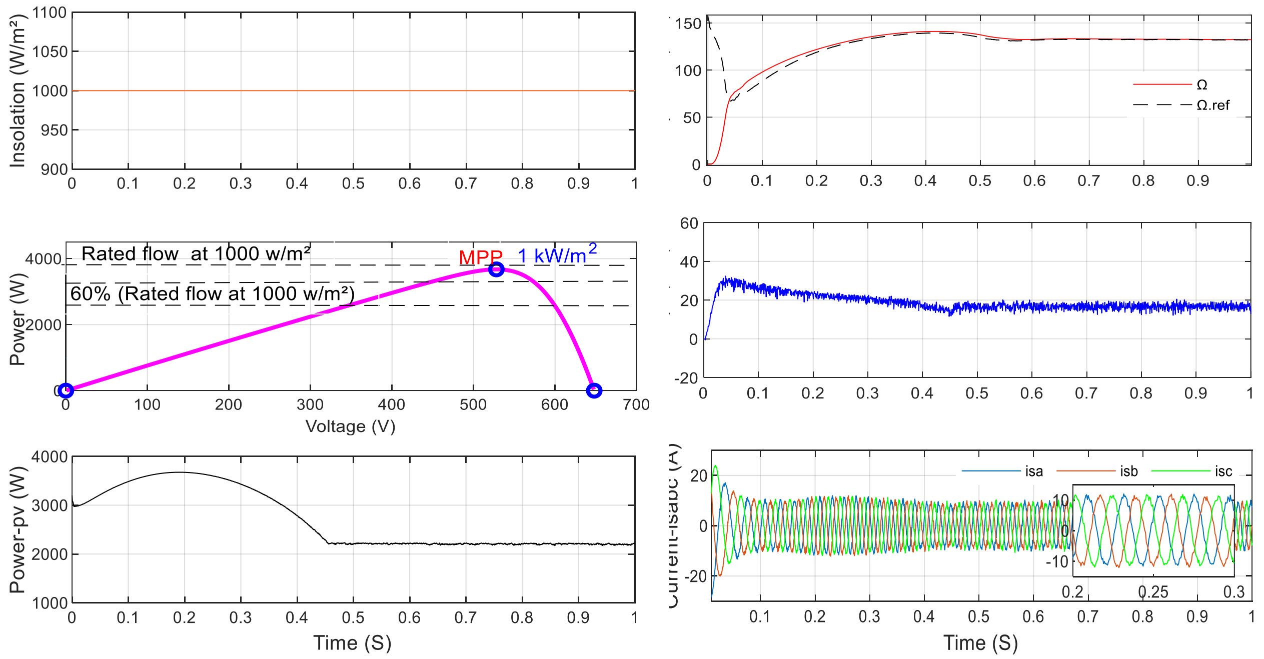

Figure 6. Dynamic performance at 60% of rated flow rate (a) PV array dynamic, (b) IM-Pump dynamic.

6. Conclusion

The performance of the integrated photovoltaic (PV) and water pumping system, employing both FS-MPC and DB-MPC, was thoroughly evaluated under varying insolation levels from 1000 W/m² to 700 W/m². The system demonstrated prompt Maximum Power Point Tracking (MPPT) at the onset of operation, stabilizing PV voltage (Vpv), current (Ipv), and power (Ppv) at the maximum power point (MPP) within a fraction of a second. The predictive control techniques effectively managed the transition from 1000 W/m² to 700 W/m² insolation, showcasing stability in Vpv and rapid adjustment in Ipv at MPP. The interconnected high-gain observer accurately estimated motor speed and facilitated the attainment of the rated rotor speed in line with the desired reference speed. DB-MPC exhibited superior dynamic response and shorter settling times compared to conventional methods. Additionally, the InC algorithm extended the photovoltaic array's operation at different points with constant insolation, highlighting a decrease in power output and corresponding adjustments in motor speed and torque to meet specific flow rate requirements. Overall, the results affirm the efficacy and adaptability of the proposed control strategies in optimizing the performance of the PV-driven water pumping system.

References

Amin, S. B., Chowdhury, M. I., Ehsan, S. A., & Iqbal, S. Z. (2021). Solar energy and natural disasters: Exploring household coping mechanisms, capacity, and resilience in Bangladesh. *Energy Research & Social Science, 79*, 102190.

Bekhoucha, N., Kermadi, M., Mesbahi, N., & Mekhilef, S. (2021). Performance investigation of deadbeat predictive controllers for three-level neutral point clamped inverter. *IEEE Journal of Emerging and Selected Topics in Power Electronics, 10*(1), 1165-1177.

Comarella, B. V., Carletti, D., Yahyaoui, I., & Encarnação, L. F. (2023). Theoretical and Experimental Comparative Analysis of Finite Control Set Model Predictive Control Strategies. *Electronics, 12*(6), 1482.

El Daoudi, S., Lazrak, L., El Ouanjli, N., & Lafkih, M. A. (2021). Sensorless fuzzy direct torque control of induction motor with sliding mode speed controller. *Computers & Electrical Engineering, 96*, 107490.

El Ouanjli, N., Mahfoud, S., Derouich, A., El Daoudi, S., & El Mahfoud, M. (2022). *Speed Sensorless Fuzzy Direct Torque Control of Induction Motor Based MRAS Method.* Paper presented at the International Conference on Digital Technologies and Applications.

Ghanes, M. (2005). *Observation et commande de la machine asynchrone sans capteur mécanique.* Ecole Centrale de Nantes (ECN); Université de Nantes.

Gupta, E. (2019). The impact of solar water pumps on energy-water-food nexus: Evidence from Rajasthan, India. *Energy Policy, 129*, 598-609.

Habibullah, M., Lu, D. D.-C., Xiao, D., & Rahman, M. F. (2016). A simplified finite-state predictive direct torque control for induction motor drive. *IEEE Transactions on Industrial Electronics, 63*(6), 3964-3975.

Jaafari, A., Davari, A., Garcia, C., & Rodriguez, J. (2022). Using vertical areas in finite set model predictive control of a three-level inverter aimed at computation reduction. *Turkish Journal of Electrical Engineering and Computer Sciences, 30*(1), 18-34.

Kanaan, H., & Al-Haddad, K. (2020). Multilevel Switching Mode Operation of Finite Set Model Predictive Control for Grid-Connected Packed E-Cell (PEC) Inverter. *IEEE Transactions on Industrial Electronics*.

Keshavarzi, M. D., & Ali, M. H. (2021). Dynamic performance enhancement of power grids by operating solar photovoltaic (PV) system as supercapacitor energy storage. *Energies, 14*(14), 4277.

Khan, K., Shukla, S., & Singh, B. (2019). Performance-based design of induction motor drive for single-stage PV array fed water pumping. *IEEE transactions on industry applications, 55*(4), 4286-4297.

Khodapanah, M., Ghanbari, T., Moshksar, E., & Hosseini, Z. (2023). Partial shading detection and hotspot prediction in photovoltaic systems based on numerical differentiation and integration of the P− V curves. *IET Renewable Power Generation, 17*(2), 279-295.

Kumar, M., Panda, K. P., Rosas-Caro, J. C., Valderrabano-Gonzalez, A., & Panda, G. (2023). Comprehensive Review of Conventional and Emerging Maximum Power Point Tracking Algorithms for Uniformly and Partially Shaded Solar Photovoltaic Systems. *IEEE Access*.

Lakshmi, M., & Hemamalini, S. (2019). Coordinated control of MPPT and voltage regulation using single-stage high gain DC–DC converter in a grid-connected PV system. *Electric Power Systems Research, 169*, 65-73.

Lammouchi, Z., & Barra, K. (2020a). Particle swarm weighting factor optimisation for predictive control of three level inverter with balanced voltages. *International Journal of Power Electronics, 12*(3), 302-316.

Lammouchi, Z., & Bekakra, Y. (2020b). *Predictive Power Control for Photovoltaic Grid Connected System with Reduction of Switching Frequency.* Paper presented at the 2020 1st International Conference on Communications, Control Systems and Signal Processing (CCSSP).

Li, H., Lin, J., & Lu, Z. (2019). Three vectors model predictive torque control without weighting factor based on electromagnetic torque feedback compensation. *Energies, 12*(7), 1393.

Luo, W., & Zhou, M. (2023). Multi-vector based model predictive control for nested neutral point piloted converters with constant switching frequency. *CPSS Transactions on Power Electronics and Applications*.

Mathew, D., & Naidu, R. C. (2023). A review on single-phase boost inverter technology for low power grid integrated solar PV applications. *Ain Shams Engineering Journal*, 102365.

Murillo-Yarce, D., Araya, B., Restrepo, C., Rivera, M., & Wheeler, P. (2023). Impact of Sequential Model Predictive Control on Induction Motor Performance: Comparison of Converter Topologies. *Mathematics, 11*(4), 972.

Naifar, O., Boukettaya, G., Oualha, A., & Ouali, A. (2015). A comparative study between a high-gain interconnected observer and an adaptive observer applied to IM-based WECS. *The European Physical Journal Plus, 130*, 1-13.

Novak, M., Xie, H., Dragicevic, T., Wang, F., Rodriguez, J., & Blaabjerg, F. (2020). Optimal cost function parameter design in predictive torque control (PTC) using artificial neural networks (ANN). *IEEE Transactions on Industrial Electronics, 68*(8), 7309-7319.

Rosas-Caro, J., & Valderrabano-Gonzalez, A. (2023). Comprehensive review of conventional and emerging maximum power point tracking algorithms for uniformly and partially shaded solar photovoltaic systems. *Repositorio Scripta; Repositorio Nacional Conacyt; Openaire*.

Sandre Hernandez, O., Cervantes-Rojas, J. S., Ordaz Oliver, J. P., & Cuvas Castillo, C. (2021). Stator Fixed Deadbeat Predictive Torque and Flux Control of a PMSM Drive with Modulated Duty Cycle. *Energies, 14*(10), 2769.

Shang, L., Guo, H., & Zhu, W. (2020). An improved MPPT control strategy based on incremental conductance algorithm. *Protection and Control of Modern Power Systems, 5*, 1-8.

Shukla, S., & Singh, B. (2020). Single-stage pv-grid interactive induction motor drive with improved flux estimation technique for water pumping with reduced sensors. *IEEE Transactions on Power Electronics, 35*(12), 12988-12999.

Singh, B., & Shukla, S. (2018). Induction motor drive for PV water pumping with reduced sensors. *IET Power Electronics, 11*(12), 1903-1913.

Su, D., Zhang, C., & Dong, Y. (2017). Finite-state model predictive current control for surface-mounted permanent magnet synchronous motors based on current locus. *IEEE Access, 5*, 27366-27375.

Traore, D., De Leon, J., & Glumineau, A. (2012). Adaptive interconnected observer-based backstepping control design for sensorless induction motor. *Automatica, 48*(4), 682-687.

Wang, C., Cao, D., Qu, X., & Fan, C. (2022). An Improved Finite Control Set Model Predictive Current Control for a Two-Phase Hybrid Stepper Motor Fed by a Three-Phase VSI. *Energies, 15*(3), 1222.

Xie, H., Wang, F., He, Y., Rodríguez, J., & Kennel, R. (2021). Encoderless parallel predictive torque control for induction machine using a robust model reference adaptive system. *IEEE Transactions on Energy Conversion, 37*(1), 232-242.

Zhang, M., Wu, Q., Chen, X., Dahhou, B., & Li, Z. (2020). Observer Design for Nonlinear Invertible System from the View of Both Local and Global Levels. *Applied Sciences, 10*(22), 7966.

Zhang, Y., & Yang, H. (2014). *An improved two-vectors-based model predictive torque control without weighting factors for induction motor drives.* Paper presented at the 2014 17th International Conference on Electrical Machines and Systems (ICEMS).1